RSC Advances

PAPER

View Article Online
View Journal | View Issue

Cite this: *RSC Adv.*, 2020, **10**, 23813

In vitro evaluation of novel low-pressure spark plasma sintered HA–BG composite scaffolds for bone tissue engineering†

Muhammad Rizwan, ‡[af] Krishnamurithy Genasan, ‡*[b] Malliga Raman Murali, [b] Hanumantha Rao Balaji Raghavendran, [b] Rodianah Alias, [c] Yi Ying Cheok, [d] Won Fen Wong, [d] Azura Mansor,[b] M. Hamdi,*[ef] Wan Jeffrey Basirun[g] and Tunku Kamarul*[b]

The low-pressure spark plasma sintering (SPS) technique is adopted to fabricate hydroxyapatite–bioglass (HA–BG) scaffolds while maintaining the physical properties of both components, including their bulk and relative density and hardness. However, prior to their orthopaedic and dental applications, these scaffolds must be validated *via* pre-clinical assessments. In the present study, scaffolds with different ratios of HA : BG, namely, 100 : 0 (HB 0 S), 90 : 10 (HB 10 S), 80 : 20 (HB 20 S) and 70 : 30 (HB 30 S) were fabricated. These scaffolds were characterized by investigating their physicochemical properties (X-ray diffraction (XRD) and surface wettability), bioactivity in a simulated body fluid (SBF) (field emission scanning electron microscopy (FESEM), Fourier-transform infrared spectroscopy (FTIR) and calcium dissolution), antimicrobial properties, biocompatibility and osteoinduction of human bone marrow-derived mesenchymal stromal cells (hBMSCs) and human monocyte immune cell response. The XRD and surface wettability results confirmed no formation of undesirable phases and the enhanced surface hydrophilicity of the scaffolds, respectively. The bioactivity in SBF indicated the formation of bone-like apatite on the surface of the scaffolds, corresponding to an increase in BG%, which was confirmed through FTIR spectra and the increasing trend of calcium release in SBF. The scaffolds showed inhibition properties against *Staphylococcus aureus* and *Staphylococcus epidermidis*. The scanning electron microscopy (SEM) micrographs and Alamar Blue proliferation assay indicated the good attachment and significant proliferation, respectively, of hBMSCs on the scaffolds. Alizarin Red S staining confirmed that the scaffolds supported the mineralisation of hBMSCs. The osteogenic protein secretion (bone morphogenetic protein-2 (BMP2), type-I collagen (COL1) and osterix (OSX)) was significant on the HB 30 S-seeded hBMSCs when compared with that of HB 0 S. The monocyte migration was significantly halted in response to HA–BG-conditioned media when compared with the positive control (monocyte chemoattractant protein-1: MCP-1). In conclusion, the HB 30 S composite scaffold has a greater potential to substitute bone grafts in orthopaedic and dental applications.

Received 12th May 2020
Accepted 3rd June 2020

DOI: 10.1039/d0ra04227g

rsc.li/rsc-advances

[a]*Department of Metallurgical Engineering, Faculty of Chemical and Process Engineering, NED University of Engineering and Technology, 75270, Karachi, Pakistan. E-mail: materialist.riz@gmail.com*

[b]*National Orthopaedic Centre of Excellence for Research & Learning (NOCERAL), Department of Orthopaedic Surgery, Faculty of Medicine, University of Malaya, 50603 Kuala Lumpur, Malaysia. E-mail: hbr_bala@yahoo.com; mrmurali08@gmail.com; azuramansor@ummc.edu.my; tkzrea@ummc.edu.my*

[c]*Department of Manufacturing Technology, Faculty of Innovative Design & Technology, University Sultan Zainal Abidin, 21030 Kuala Terengganu, Malaysia. E-mail: rodianahalias2112@gmail.com*

[d]*Department of Medical Microbiology, Faculty of Medicine, University of Malaya, 50603 Kuala Lumpur, Malaysia. E-mail: heathercheok@gmail.com; wonfen@um.edu.my*

[e]*Chancellery Office, The National University of Malaysia, 43600 Bangi, Selangor, Malaysia*

[f]*Centre of Advanced Manufacturing and Material Processing, University of Malaya, 50603 Kuala Lumpur, Malaysia. E-mail: hamdi@um.edu.my*

[g]*Department of Chemistry, Faculty of Science, University of Malaya, 50603 Kuala Lumpur, Malaysia. E-mail: jeff@um.edu.my*

† Electronic supplementary information (ESI) available: (1) Ball-milled bioglass particle size distribution, elemental mapping of HB 20 S and XRD pattern of bioglass. *In vitro* bioactivity analysis on HB 0 S, confocal images of the osteogenic intra- and extra-cellular proteins secreted on the periphery of the HA–BG composite scaffold-seeded hBMSCs, and Haematoxylin and Eosin (H&E) stained insert membranes (IM) retrieved after 3 h migration assay. Post analysis of bright-field images of migrated monocytes using Image-J analysis tool with an established plugin (PDP). (2) Raw data from the experimental outcomes (Excel). See DOI: 10.1039/d0ra04227g

‡ M. R. and K. G. contributed equally.

1 Introduction

Hydroxyapatite (HA), a predominant mineral component of bones, has been widely used as a substitute for bone grafts in orthopaedic and/or dental applications.[1] It has an inherent capacity to exhibit osteoconduction, thus allowing the migration of host bone-forming cells into the scaffold to slowly replace it with new bones over time.[2] However, the major limitations of HA-derived scaffolds are their poor antimicrobial and osteoinductive properties.[3] There have been attempts to overcome these limitations by incorporating HA with either carbon nanotubes (CNTs)[4] or graphene.[5] Nonetheless, the issues associated with its osteoinductive properties are yet to be solved. Accordingly, bioactive glass (BG) has become one of the options since it inhibits the formation of biofilms, which are primarily produced by *Pseudomonas aeruginosa*.[6] In addition, it supports the osteogenic differentiation of stem cells and creates a strong bonding with the bone at the interface *via* the induction of HA formation.[7] However, its poor strength, toughness and ductility and calcium phosphate (CaP) content resembling the human bone characteristic hinder its extensive use in bone tissue engineering.[8]

A recent finding from our team demonstrated that the fabrication of composite scaffolds comprising HA and BG® 45S5 using the low-pressure spark plasma sintering (SPS) technique was successful.[9] This attempt was primarily made to avoid severe chemical reactions between the precursors and to produce scaffolds with desirable hardness and density.[3] It was confirmed that the composition of these scaffolds was only CaP and adequate glassy phases. This appropriate amount of glassy pockets provides a significant resistance against deformation from the penetration of a Vickers indenter through the CaP-rich phase, which leads to an enhanced hardness.[9] However, prior to use in pre-clinical animal studies or clinical trials, these novel scaffolds must be validated for their *in vitro* bioactivity, antimicrobial, biocompatibility, osteogenic differentiation properties and resistance to the immune cell response.

Bacterial strains such as *Staphylococcus* species (spp.) are important Gram-positive bacteria, which are the main cause of premature orthopaedic and dental implant failure.[10] Thus, it is crucial to understand the inhibition activity of novel composite scaffolds against these methicillin-resistant and sensitive strains. Consequently, their role in preventing biofilm formation during post-surgery recovery can be guaranteed. Besides that, the assessments of *in vitro* biocompatibility and osteoinductive properties of new scaffolds are also prerequisite steps. Accordingly, the osteoblast precursor, which is mesenchymal stromal cells (MSCs), becomes the best selection.[11] MSCs have an inherent characteristic to undergo osteogenic differentiation to become bone-forming cells such as osteoblasts.[12,13] In pathophysiological conditions such as in bone fracture, MSCs tend to migrate to the area of inflammation, which occurs due to fracture, and differentiate, becoming osteocytes and causing bone mineral deposition to repair the defects.[14] Therefore, incorporating MSCs in biomaterial scaffolds have become a common approach since it can enhance the reparative process, supporting the host MSCs.[15] However, biomaterial scaffolds are still deemed as foreign bodies to the recipient inert immune cells such as macrophages and monocytes. These cells will get activated and release inflammatory mediators such as tumor necrosis factor-alpha (TNF-α) and interleukin-6 (IL-6) if the scaffolds/implants elicit a foreign body reaction.[16] These mediators are responsible for the migration of circulating monocytes from peripheral blood and formation of osteoclasts, implicating osteolysis at the bone–implant interface and premature failure of implants. Therefore, evaluating bone tissue constructs/scaffolds for their resistance to monocyte migration in an *in vitro* environment is essential.

Since novel SPSed (low-pressure spark plasma sintered) HA–BG composite scaffolds have emerged as potential candidates for bone tissue engineering, their application requires pre-clinical assessments. Furthermore, a foreign body reaction under *in vitro* conditions to mimic the physiological microenvironment at the bone–implant interface is worth exploring. Thus, the present study was designed to investigate the properties of SPSed HA–BG composite scaffolds, including their physicochemical characteristics, methicillin resistant (*S. aureus*) and sensitive (*S. epidermidis*) *Staphylococcus* spp. inhibition ability, human bone marrow-derived mesenchymal stromal cell (hBMSC) adhesion, proliferation and osteogenic differentiation promoting properties, and monocyte migration-resisting behaviour.

2 Materials and methods

2.1 Fabrication of HA–BG composite scaffolds

Bioglass (BG) powder (5–10 μm) was obtained by ball milling BG spheres, which were procured from XL SciTech Inc., USA. HA submicron powder (Cod. 21223) was supplied by Sigma Aldrich, Malaysia. The premixed compositions were prepared using polyethylene ball mill jars by adding 10, 20 and 30 wt% BG to HA. The sample containing pure HA (H) without BG (B) was identified as HB 0, whereas the composite samples containing 10, 20 and 30 wt% BG were designated as HB 10, HB 20 and HB 30, respectively. Very low-pressure consolidation of the premixed powders was performed at 1000 °C through spark plasma sintering (SPS-1030S, SPS Syntex system, USA) under a vacuum pressure of 5 Pa. A 30 mm diameter graphite die was filled with 8 g premixed composition and sintered for 30 min at a heating rate of 50 °C min^{-1}. Initially, a pressure of 1.83 MPa was applied to ensure the current passage until the temperature reached 1000 °C. The final load reached 3.67 MPa during the sintering process. After 30 min of sintering, the samples were allowed to cool under the same load and vacuum conditions.[9] The sintered scaffolds were then identified as HB 10 Sintered (S), HB 10 S, HB 20 S and HB 30 S, respectively. The tablets were then cut into various sizes using a diamond cutter to support different experiments in the study. The SPSed HA–BG composite scaffolds were sterilized using 25 kGy gamma irradiation at the Nuclear Agency of Malaysia prior to their used in the *in vitro* bioactivity, antimicrobial, hBMSC cell culture and monocyte immune response experiments.

2.2 Physicochemical characterisation

The XRD patterns of the scaffolds were recorded on an XRD-6100 X-ray diffractometer (Shimadzu, Japan) using Ni-filtered monochromatized CuKα radiation (k = 1.54056 Å) at 40 kV and 30 mA with a step size of 0.02° and a scanning rate of 2° min^{-1} in the 2θ range of 10° to 80°. Microstructural analyses were carried out on a high-resolution field emission scanning electron microscope (FESEM) (FEI Quanta 200F, US) and tabletop SEM (Phenom ProX, Netherlands). Prior to the SEM/FESEM analyses, the ground and polished samples were coated with a thin layer of platinum (Pt)/gold (Au) to avoid charging effects. The chemical composition of the phases was determined using an energy dispersive X-ray analyser (EDAX) attached to the FESEM/tabletop SEM. Surface hydrophilicity or wettability is one of the influential parameters to control cell attachment *via* protein adsorption.[17] The contact angle between a liquid and solid surface is used as a scale to measure the level of wetting. The wettability of the scaffolds was analysed using a sessile Easy DROP instrument (OCA 15EC; Data Physics Instruments GmbH; Germany). The liquid volume and dropping velocity were fixed at 10 μL and 2 μL s^{-1}, respectively. The particle distribution of the BG was measured using a laser particle analyser (Mastersizer 3000, UK).

2.3 *In vitro* bioactivity analysis

The *in vitro* bioactivity analysis was performed to examine the formation of bone-like apatite on the samples in SBF using a published protocol.[18] The pH of 7.4 and ion concentration (Na^+: 142.0, K^+: 5.0, Mg^{2+}: 1.5, Ca^{2+}: 2.5, Cl^-: 147.8, HCO^{3-}: 4.2, $HPO_2{}^{4-}$: 1.0, and $SO_2{}^{4-}$: 0.5 mM) of SBF are comparable to that of human blood plasma. Briefly, SBF was prepared by dissolving reagent-grade mixtures of $CaCl_2$, $K_2HPO_4{\cdot}3H_2O$, KCl, NaCl, $MgCl_2{\cdot}H_2O$, $NaHCO_3$ and Na_2SO_4 in double distilled water (ddH_2O) and adjusting the pH to 7.4 using Tris and hydrochloric acid (HCl). The as-sintered samples were soaked in SBF stored in polyethylene beakers and incubated at 37 °C for 7 days. The volume of SBF required for the different samples was calculated using a published equation[18] as follows:

$$V_s = \frac{S_a}{10} \quad (1)$$

where V_s is the volume of SBF in mL and S_a is the surface area of the sample in mm^2.

The SBF was refreshed every 48 h to maintain the homogenous ion concentration. Microstructural analysis was then performed on the soaked samples using FESEM (Hitachi SU 8220, Japan) and the chemical composition of the precipitated HA was confirmed using EDAX. For the FTIR measurements, the scaffolds were crushed and pressed to obtain thin circular wafers and transmission spectra were recorded in the wavenumber range of 2000–400 cm^{-1} (Perkin Elmer Spectrum 400, US).

2.4 *In vitro* resorption analysis

Understanding the biodegradation rate of a calcium phosphate (CaP)-based scaffold is an essential step to determine its sustainability in a defect region, while promoting neo-bone formation.[19] Furthermore, it has been reported that an optimized biodegradation rate of a scaffold can boost bone tissue regeneration through immunomodulatory activity.[20] In the present study, the resorption behaviour of the SPSed HA–BG composite scaffolds was measured *via in vitro* biodegradation analysis. The biodegradation test was performed in Ca-free Tris-based electrolyte using the protocol adopted from the literature.[20] Briefly, 0.05 M Ca-free Tris-based electrolyte buffer was prepared by dissolving 6.057 g Tris and the pH was adjusted to 7.3 ± 0.05 using weak HCl. The composite samples were then soaked in 200 mL of Tris buffer under non-contact stirring at 200 rpm and incubated at 37 °C for 5 h. The buffer was then collected, and its calcium content detected using atomic absorption spectroscopy (AAS) (iCE 3000, USA).

2.5 Antimicrobial activity

Antimicrobial testing of the SPSed HA–BG composite scaffolds was carried out on both methicillin-sensitive and resistant *Staphylococcus* spp. as described previously with minor modifications.[21] *Staphylococcus aureus* (ATCC 1749 and ATCC 811) and *Staphylococcus epidermidis* (ATCC 700593 and ATCC 35984) were purchased from American Type Culture Collection (ATCC) and maintained on nutrient agar at 37 °C in a humidified incubator. Prior to the experiment, each strain was inoculated in 3 mL Luria–Bertani (LB) broth (Difco, UK) and cultured at 37 °C on a shaker at 2500 rpm for 24 h. Absorbance measurements were performed for each strain at OD_{600} and adjusted to approximately 0.5 McFarland turbidity standard. Additionally, 25 mg of each compound was weighed and incubated with 1 mL of LB broth for 1 h at 37 °C on a shaker at 2500 rpm. Then, the *Staphylococcus* spp. strains were inoculated directly in the pre-incubated LB broth at 1 : 50 dilution and incubated at 37 °C on a shaker at 2500 rpm for 24 h. Subsequently, serial dilutions of the reaction mixture were plated on nutrient agar and colony-forming units (CFUs) were counted after 24 h. The results are expressed as mean $\log_{12}$ colony forming unit (CFU) with standard deviation (SD).

2.6 Isolation and culture of human bone marrow mesenchymal stromal cells (hBMSCs)

Ethics approval was granted by the University of Malaya Medical Centre (UMMC) Ethics Committee (Ethics No.: 20164-2398) to obtain patient bone marrow and peripheral blood samples. The bone marrow aspirates and/or peripheral blood of patients (aged 50 to 70 years) were collected after obtaining written consent from individuals undergoing total knee replacement. The purification of human bone marrow mesenchymal stromal cells (hBMSCs) was performed using the standard Ficoll-Paque gradient centrifugation (density 1.073 g mL^{-1}) according to the manufacturer's instructions (GE Healthcare Bio-Sciences, US). The density gradient centrifugation was performed for 25 min at 2200 rpm. The central layer containing mononuclear cells was isolated and washed thrice with phosphate-buffered saline (PBS) (1×) (Gibco, Invitrogen, US). The cell culture was carried out in low glucose Dulbecco modified Eagles' medium (DMEM,

Invitrogen, US) supplemented with 10% fetal bovine serum (FBS, Invitrogen), 100 U mL^{-1} penicillin (Sigma-Aldrich, US) and 100 mg mL^{-1} streptomycin (Sigma-Aldrich). The number of cells and their viability were determined using the Trypan blue exclusion method. Almost 1×10^6 cells were seeded on the T-75 culture and then incubated at 37 °C in 5% CO_2 with 95% humidity. For the subsequent passaging, the cells in passage-0 (P_0), having reached 80% confluency, were then washed using PBS (1×) and later incubated in trypsin (TrypLE, Gibco) for 3 min in a CO_2 incubator at 37 °C for complete cell detachment. The harvested P_0 cells were sub-cultured again in passage-1 (P_1) and the culture medium was changed every 72 h.

2.6.1 Cell seeding on the SPSed HA–BG composite scaffolds. The hBMSCs were enzymatically separated using 3 mL of trypsin upon reaching 80% confluency at P_1. A cell suspension was prepared and seeded on the SPSed HA–BG composite scaffolds in a forty-eight-well low attachment plate dropwise at a density of 1×10^6 cells per mL. The scaffolds without cells were used as a negative control. All the scaffolds were then maintained in DMEM supplemented with 10% FBS and incubated at 37 °C in 5% CO_2 with 95% humidity.

2.6.2 Cell attachment analysis. Scanning electron microscopy (SEM) analysis was performed to observe the surface attachment behaviour of the hBMSCs ($n = 3$) seeded on the SPSed HA–BG composite scaffolds. The cell-seeded scaffolds at day 21 were fixed overnight in 4% glutaraldehyde in 0.1 M cacodylate buffer and post-fixed for 1 h in 1% aqueous osmium tetroxide. The scaffolds were then washed twice using double-distilled water (ddH_2O) for 10 min/step prior to use in the serial dehydration process involving multiple steps. The serial dehydration steps were performed by soaking the scaffolds in 30%, 50%, 70%, 80%, 90%, 95% and 100% (twice) ethanol for 15 min/step. An intermediate drying step was performed using ethanol and acetone at the ratio of 3 : 1, 1 : 1 and 1 : 3 for 15 min per step. The final dehydration was performed thrice in pure acetone for 20 min per step. The scaffolds were then dried at a critical point using critical point drier (Bal Tec, CPD030, Finland). The scaffolds were mounted on aluminium stubs and coated with gold using a sputter deposition system prior to examination using a tabletop scanning electron microscope (Phenom ProX, USA). The SEM micrographs of the scaffolds were obtained at 400× and 3000×.

2.6.3 Cell proliferation analysis. The effect of the SPSed HA–BG composite scaffolds ($n = 3$) on cell proliferation was evaluated using the colorimetric indicator Alamar Blue (AB) cell proliferation/viability assay (Gibco). The assay was carried out by analysing the AB reduction on day 1, 3, 7, 14 and 21. AB was directly supplemented in the culture media of all the scaffolds at the final concentration of 10%, and then incubation was carried out for 10 h. About 100 μL of medium of each scaffold was moved to a 96-well plate in triplicate. AB was added to the scaffolds without cells as a blank. The 96-well plate was subjected to absorbance reading at 570 nm and 600 nm (reference wavelength) using a microplate reader (Epoch, US). These absorbance readings were substituted in an equation provided by the manufacturer (Invitrogen) to measure AB percentage of reduction. The results acquired were averaged and presented as mean ± SD.

2.6.4 Mineralisation. Alizarin Red (AR) S staining and calcium (Ca) quantification were performed on the cell-seeded SPSed HA–BG composite scaffolds to monitor the level of mineralisation at day 20 using a published protocol with minor modification.[22] The scaffolds without cells were used as a baseline control. Briefly, the scaffolds were fixed with pure methanol for 10 min and subsequently washed with sterile ddH_2O prior to incubation with 0.1% AR S Tris–HCl solution at 37 °C for 30 min. The scaffolds were then thoroughly rinsed with ddH_2O to remove the excess AR S and dried before imaging. About 10 visual fields were randomly selected and a representative image was used for presentation. To further confirm the elements of the minerals secreted by the cells seeded on the SPSed HA–BG composite scaffolds, EDAX was performed on the extracellular matrix (ECM) found on the periphery of the cells with the assistance of real-time SEM observation.

2.6.5 Biochemical analysis

2.6.5.1 Alkaline phosphatase assay. Alkaline phosphatase (ALP) activity was measured in the culture media of the cell-seeded SPSed HA–BG composite scaffolds collected on day 5, 10, 15 and 20 using an ALP colorimetric assay kit (BioVision, USA). The culture media from the scaffolds without cells were used as background controls. 50 μL of media from the cell-seeded scaffolds ($n = 3$) in duplicate was mixed with 30 μL of *para*-nitrophenyl phosphate (*p*NPP) substrate. The aspirates were then added with assay buffer solution to make a final volume of 130 μL and incubated for 60 min at 25 °C in the dark. Sample background controls were also prepared using the same method described above. 20 μL of stop solution was added to all the background controls before the 60 min incubation period, except for all the aspirates, which were added upon completion of the incubation period. The absorbance of the aspirates and background controls was measured at a wavelength of 405 nm using a microplate reader (Epoch). The optical density values for each calibrator against the corresponding concentration of ALP were plotted to produce a standard curve. The ALP concentration in the aspirates was extrapolated using the linear equation obtained from the above standard curve. Statistical analysis was performed between days (day 5, baseline control) and groups (HB 0 S, baseline control) using the Mann–Whitney and Kruskal–Wallis tests in SPSS. The assessments were reported to be statistically significant if $p < 0.05$.

2.6.5.2 Osteocalcin assay. The osteocalcin (OC) assay was performed on the culture media of the cell-seeded SPSed HA–BG composite scaffolds collected on day 5, 10, 15 and 20 using a human OC enzyme-linked immunosorbent assay (ELISA) kit (IBL International, Germany). The culture media from the scaffolds without cells were used as background controls. The wells from the primary antibody-coated 96-well ELISA microtiter plate were selected and secured in a holding frame. 25 μL of calibrator, background control and aspirate (culture media of cell-seeded SPSed HA–BG composite scaffolds) were pipetted into the appropriate wells. Then an aliquot of 100 μL working organic solute transporter beta antibody (anti-OST) horseradish peroxidase (HRP) conjugate was added to all the wells. The plate was

then incubated for 2 h at room temperature (RT). The supernatant was discarded, and the wells were washed thrice with 400 μL of washing buffer. An aliquot of 100 μL chromogenic solution was added to all the wells within 15 min of the washing step and incubated for 30 min at RT. The plate was then used for absorbance reading at 450 nm using a microplate reader (Epoch). A standard curve was plotted using the optical density values of the calibrator against the corresponding OC concentration. The OC concentration in the aspirates was extrapolated using the linear equation drawn from the standard curve. Statistical analysis was performed between days (day 5, baseline control) and groups (HB 0 S, baseline control) using the Mann–Whitney and Kruskal–Wallis tests in SPSS. The assessments were reported to be statistically significant if $p < 0.05$.

2.6.6 Immunocytochemistry (ICC). For immunofluorescence staining, the cell-seeded SPSed HA–BG composite scaffolds and scaffolds without cells (negative control) were fixed on day 21 with 4% (w/v) paraformaldehyde (PFA) (Sigma, US) in PBS (1×) (pH = 7.4) for 15 min at RT. The scaffolds were then washed with PBS (1×) and incubated with 1% bovine serum albumin (BSA), 22.52 mg mL^{-1} glycine in PBS + 0.1% Tween 20 (PBST) for 30 min to avoid false binding of the antibodies. For primary antibody staining, bone morphogenetic protein-2 (BMP2) (anti-BMP2 antibody [IgG]) (1 μg mL; Abcam, UK), type-I collagen (Col1) (anti-collagen 1 antibody [IgG1]) (1/1000; Abcam) and osterix (OSX) (anti-Sp7/osterix antibody [IgG]) (1/1000; Abcam) were used. The scaffolds were incubated in diluted mouse primary antibody in a humidified chamber for 1 h at RT. The solution was then discarded, and the samples were washed thrice with PBS (1×). For secondary antibody staining, chicken polyclonal secondary antibody conjugated with Alexa Fluor 647 (1 : 500; Abcam) was used. The scaffolds were incubated with secondary antibody in 1% BSA for 1 h at RT in the absence of light. The solution was then discarded, and the samples were washed thrice with PBS (1×). Prior to viewing, the samples were counterstained with Hoechst 33342 nucleic acid staining. The fluorescence signals were observed using confocal laser scanning microscopy (CLSM) with X20/0.40NA objective lens and the images were analysed with the Leica Application Suite X (LAS X, UK) imaging software. The total fluorescence intensity on the confocal images was measured using the Image-J analysis software (IJ 151j/Java 1.8.2-64 bit, NIH, US). Three random regions of interest (ROI) were assigned for each interrogation and the corrected total cell fluorescence (CTCF) was calculated using the following formula:[23]

$$\text{CTCF} = \text{integrated density} - (\text{area of selected ROI} \times \text{fluorescence of background reading}) \quad (2)$$

where the integrated density and fluorescence of background reading are in arbitrary units (A.U.) and area of selected ROI in mm^2. The data are presented as mean ± SD.

2.7 Isolation of human peripheral blood mononuclear cells (hPBMNCs)

30 mL of intravenous blood was drawn in trisodium citrate solution tubes (BD Bioscience, US) from patients ($n = 3$) undergoing total knee replacement. The whole blood (WB) was centrifuged at 1000 rpm for 10 min continuously. The plasma layer was removed, and the blood pellet was diluted with an equal volume (1 : 1) of RPMI 1640 medium (Sigma, US). The cell suspension was laid on Ficoll-Paque (density 1.073 g mL^{-1}) according to the manufacturer's instructions (GE Healthcare Bio-Sciences, US). The layer was centrifuged at 1600 rpm for 10 min at RT continuously. The hPBMNCs were recovered from the interphase and washed twice with RPMI 1640 medium. The cell pellet was suspended in macrophage serum-free medium (SFM; Gibco) and the cell density was identified using the haemocytometer cell counting technique. The hPBMNCs were either seeded on the SPSed HA–BG composite scaffolds or used in the migration assay.

2.7.1 Preparation of SPSed HA–BG composite scaffold-conditioned media. About 1×10^8 cells per mL were seeded on the scaffolds and incubated in 1 mL of SFM for 1 h at 37 °C in 5% CO_2 with 95% humidity to enrich the adherent cells (monocytes) on the scaffold. The monocyte-enriched SPSed HA–BG composite scaffolds were washed twice using sterile warm PBS (1×) to remove non-adherent cells and replenished with 1 mL of SFM prior to incubation overnight at 37 °C in 5% CO_2 with 95% humidity to prepare the SPSed HA–BG composite scaffold-conditioned media. The SPSed HA–BG composite scaffold-conditioned media were then collected, labelled as HB 0 S-conditioned media (HB 0 S-CM), HB 10 S-conditioned media (HB 10 S-CM), HB 20 S-conditioned media (HB 20 S-CM) and HB 30 S-conditioned media (HB 30 S-CM) and stored at −80 °C until they were used in the migration assay.

2.7.2 Transwell migration of monocytes. Prior to migration, all the SPSed HA–BG composite scaffold-conditioned media were centrifuged at 4000 rpm and their supernatants were collected. About 1 mL of monocyte chemoattractant protein-1 (MCP-1, 100 ng mL^{-1}), HB 0 S-CM, HB 10 S-CM, HB 20 S-CM and HB 30 S-CM were added in triplicate to a 12-well plate and the plate was inserted with a transwell. Freshly isolated hPBMNCs were added to the transwell attached with a 3 μm pore diameter transparent polyethylene terephthalate (PET) insert membrane (IM) (Greiner Bio-One, UK) using a 1 mL large tip opening serological pipette to avoid artificial activation of monocytes. The plates were incubated for 3 h at 37 °C in 5% CO_2 with 95% humidity. The insert membranes were harvested and the cells from the apical site were removed using cotton swabs. The IM was rinsed with PBS (1×), fixed using methanol and stained with H&E to observe the cells that invaded its basolateral site. The cover-slipped IM was scanned using a digital slide scanner (3DHISTECH, Hungary) and six random spots at 40× magnification on the IM for each group were captured using CaseViewer 2.3 (3DHISTECH, Hungary). The monocytes that were identified on the random spots of the IM were calculated and graphed. The migrated cells in the bottom of the triplicate wells were imaged using an inverted light microscope (Eclipse Ti-E, Nikon, UK) and the cells were calculated using the Image-J analysis software (IJ 151j/Java 1.8.2-64 bit, NIH, US).

3 Results and discussion

3.1 Physicochemical characteristics

The XRD analysis confirmed the earlier reported ability of the novel set of processing parameters to avoid the intensive chemical reaction between HA and BG and the crystallization of BG.[9] Upon sintering pure HA (containing a small amount of $CaHPO_4$), all the HA transformed to beta tricalcium phosphate (β-TCP) with a negligible amount of $CaHPO_4$, as reported by Cuccu *et al.*[24] $CaHPO_4$ transforms to calcium pyrophosphate (CPP, $Ca_2P_2O_7$) upon exposure to a temperature of around 450 °C, contributing to the formation of β-TCP.[25] In addition, the higher temperature and longer sintering time may allow the complete transformation of HA into β-TCP. With the addition of 10, 20 and 30 wt% BG, no undesirable phases were formed, contrary to the findings of other researchers using HA–BG systems.[26,27] A combination of only β-TCP and HA was achieved, exhibiting an increasing trend for HA with an increase in BG content at the expense of β-TCP. The possible mechanism behind this finding is discussed meticulously.[9] For the purpose of quantitative comparison, the highest intensity planes of HA and β-TCP in the respective reference files were calculated as the ratio of HA/β-TCP. The matching reference file and highest intensity plane *d*-spacing for HA is 96-101-1243 and $d = 2.812$, while that for β-TCP is 00-009-0169 and $d = 2.880$, respectively. The HA/β-TCP ratio for HB 0 S was 0, while it was 0.208 for HB 10 S, 4.51 for HB 20 S and 5.61 for HB 30 S. The increase in the HA/β-TCP ratio can be seen in Fig. 1 for the samples containing a higher content of BG.

The microstructural analysis of a scaffold is crucial to understand its response to processing steps, such as heat treatment.[28] The microstructural analysis of the HB 0 S sample provided visual evidence of the formation of single-phase β-TCP, which was also confirmed by the XRD analysis (Fig. 1b). The blackish region observed in the microstructure of the HB 0 S sample indicates the presence of a porous region. The glassy

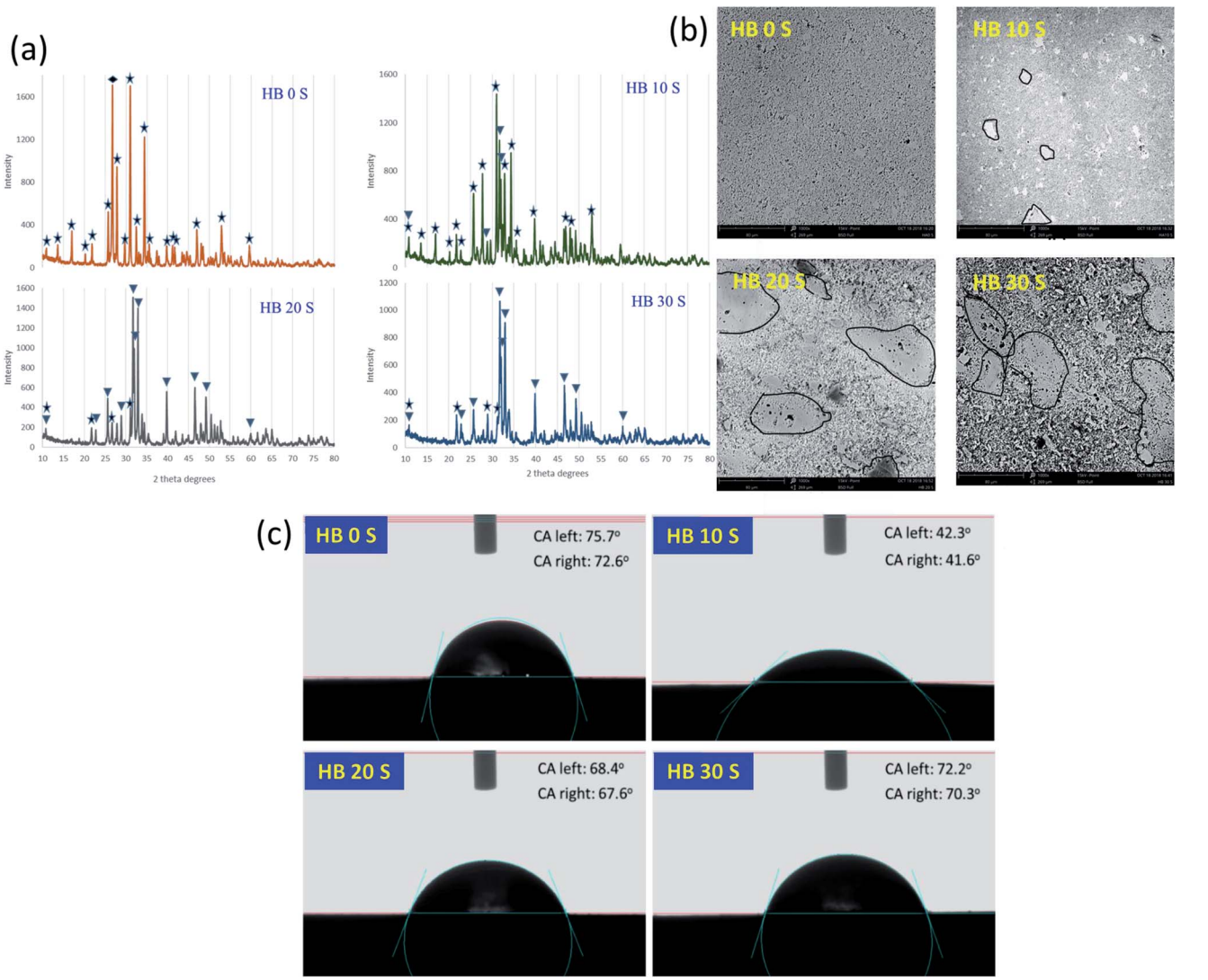

Fig. 1 Physicochemical characterisation of HB 0 S, HB 10 S, HB 20 S and HB 30 S. (a) XRD pattern, (b) microstructural analysis and (c) wettability/contact angle (CA) analysis. XRD reference pattern: $CaHPO_4$ (ICOD 00-001-0653), β-TCP (ICOD 00-009-0169) and HA (96-900-1234/96-101-1243).

region, as indicated by the black outline in the SEM images of the SPSed HA–BG composite scaffolds, was formed upon the addition of BG, which possessed various particle sizes (Fig. S1a†). In addition, it is worth noting that the CaP phase exhibited a relatively higher porosity/rough morphology with an increase in the BG content in the SPSed HA–BG composite scaffolds. This rough morphology is an indication of the huge discrepancy in the hardness of the glassy region and CaP region. Therefore, grinding and polishing could not produce scaffolds with a smooth surface.

The presence of a glassy region and CaP phases was further confirmed using elemental mapping of the HB 20 S scaffold as a representative SPSed composite scaffold (Fig. S1b†). The overlapping elemental mapping of P, Ca, Si and Na is shown in Fig. S1b.† It was found that Si (Fig. S1b†) and Na (Fig. S1b†) were the major glass-forming elements in HB 20 S. The presence of Si and Na confirms the diffusion of Na and Si in the CaP phase, which is considered responsible for the stabilization of HA with an increase in BG content.[29] BG is also composed of Ca (Fig. S1b†) and P (Fig. S1b†), but the content of these elements was considered limited. On the other hand, the CaP phase exhibited some contrast for Si and Na and very strong signals for Ca and P. To confirm the composition of BG, milled BG was SPSed under the same processing parameters, which yielded the characteristic peaks for crystalline BG ($Na_2CaSi_2O_6$: reference pattern 01-077-2189), as presented in Fig. S1c.†

Enhanced surface wettability is one of the prerequisite characteristics for biomaterial scaffolds since it augments protein absorption from the body fluid when it is implanted. This protein absorption is important to help scaffolds in supporting the attachment of surrounding local cells.[31] In the present study, the contact angle (CA) analysis revealed the wettability characteristics of the SPSed HA–BG composite scaffolds. HB 0 S exhibited the lowest wettability, which seemed to be sufficient for cell attachment compared with the other sample groups, which is consistent with a previous finding.[32] This may be primarily due to its high relative density (R.D $\sim$ 92.2%). With the addition of BG, the porosity was found to significantly increase for HB 10 S (R.D $\sim$ 88.2%), which may be the reason for its highest wettability (Fig. 1c). The further addition of BG yielded an improved density, resulting in a proportional decrease in wettability for HB 20 S (R.D $\sim$ 90.75%) and HB 30 S (R.D $\sim$ 93.9%). Interestingly, the wettability of HB 30 S was almost identical with that of HB 0 S. HB 30 S exhibited the lowest porosity among the sample groups. Thus, it can be inferred that the SPS technique maintained the wettability of the SPSed HA–BG composite scaffolds without affecting their surface hydrophilicity for optimal protein adsorption. However, other factors also have to be considered, including surface roughness, grain size, and porosity, when assessing the surface hydrophilicity of biomaterial scaffolds.[33]

3.2 *In vitro* bioactivity properties

The *in vitro* immersion of scaffolds in SBF is one of the most reliable techniques to understand their adaptation in the physiological environment of the human body. This can be assessed based on the formation of carbonated apatite (bone-like apatite layer) on the surface of the scaffolds.[34,35] In the present study, the formation of a biomimetic-hydroxyapatite layer with a cauliflower-like appearance was observed on the surface of the SPSed HA–BG composite scaffolds (Fig. 2a). The morphology of the developed apatite layer was very similar for all the samples. The thick, visibly cracked apatite layer was formed after 7 days of immersion in SBF. The developed apatite layer on all the samples exhibited almost a similar cauliflower-like morphology and porous bone-like apatite. Upon close inspection, it was observed that the blisters of apatite layer on HB 30 S were bigger compared to that on HB 20 S, and a similar pattern was also recognised between HB 20 S and HB 10 S. This indicates that the apatite layer on the samples containing a higher amount of BG was in the more mature phase of apatite formation in comparison to the composites with a lower BG content and pure HA. The formation of apatite on the surface of the CaP-based scaffolds incorporated with bioactive glass occurred through a sequence of chemical reactions when immersed in SBF, as clearly shown in the schematic illustration by Md Towhidul *et al.*[36]

This new apatite phase on the scaffolds was further confirmed *via* FTIR spectroscopy (Fig. 2b). The FTIR spectra validated the chemical compositions of the biomimetic-hydroxyapatite at different wavelengths including 550 and 660 cm^{-1} ($V_4^{\cdot}$ PO_4^{3-}), 1050 cm^{-1} ($V_3^{\cdot}$ PO_4^{3-}), 870 cm^{-1} (C–O) and 1630 cm^{-1} ($V_2^{\cdot}$ O–H). This finding is consistent with the biomimetic-hydroxyapatite growth observed on the functionalised surfaces of Ti–6Al–4V and Ti–Zr–Nb alloys.[37] However, some of the cracks and pores that were observed on the scaffolds after removal of the samples from the SBF solution may be solely due to the drying step.[38]

BG exhibited the highest bioactivity, which is primarily due to its high Ca dissolution rate.[30] As a general finding, the Ca dissolution rate of the SPSed HA–BG composite scaffolds increased with an increase in BG content (Fig. 2c). The BG was treated under similar SPSed processing conditions to investigate its Ca dissolution behaviour, which generated a dense (R.D $\sim$ 98%) disk with a much higher Ca dissolution in comparison to that of pure HA (R.D $\sim$ 92%). However, interestingly HB 30 S exhibited a 1.1-fold increase in Ca dissolution compared with that of the pure BG. The reason for this observation is still unclear.

Elemental analysis was performed on the apatite layer formed on the surface of the HB 0 S scaffold (representative) using EDAX. The FESEM image illustrates the apatite layer on the scaffold formed on day 7 after immersion in SBF (Fig. S2a†). The EDAX spectra confirmed the formation of a CaP phase on the scaffold with a minute content of Na, Mg and Cl (Fig. S2b†). The Ca/P ratio of the developed apatite layer was between 1.4 and 1.65, which closely resembles 1.67, the ideal Ca/P ratio of HA.[39]

3.3 Antimicrobial effect of SPSed HA–BG composite scaffolds

Pure bioactive glass powder was shown to inhibit the growth of all *Staphylococcus* spp., although significant inhibition was only

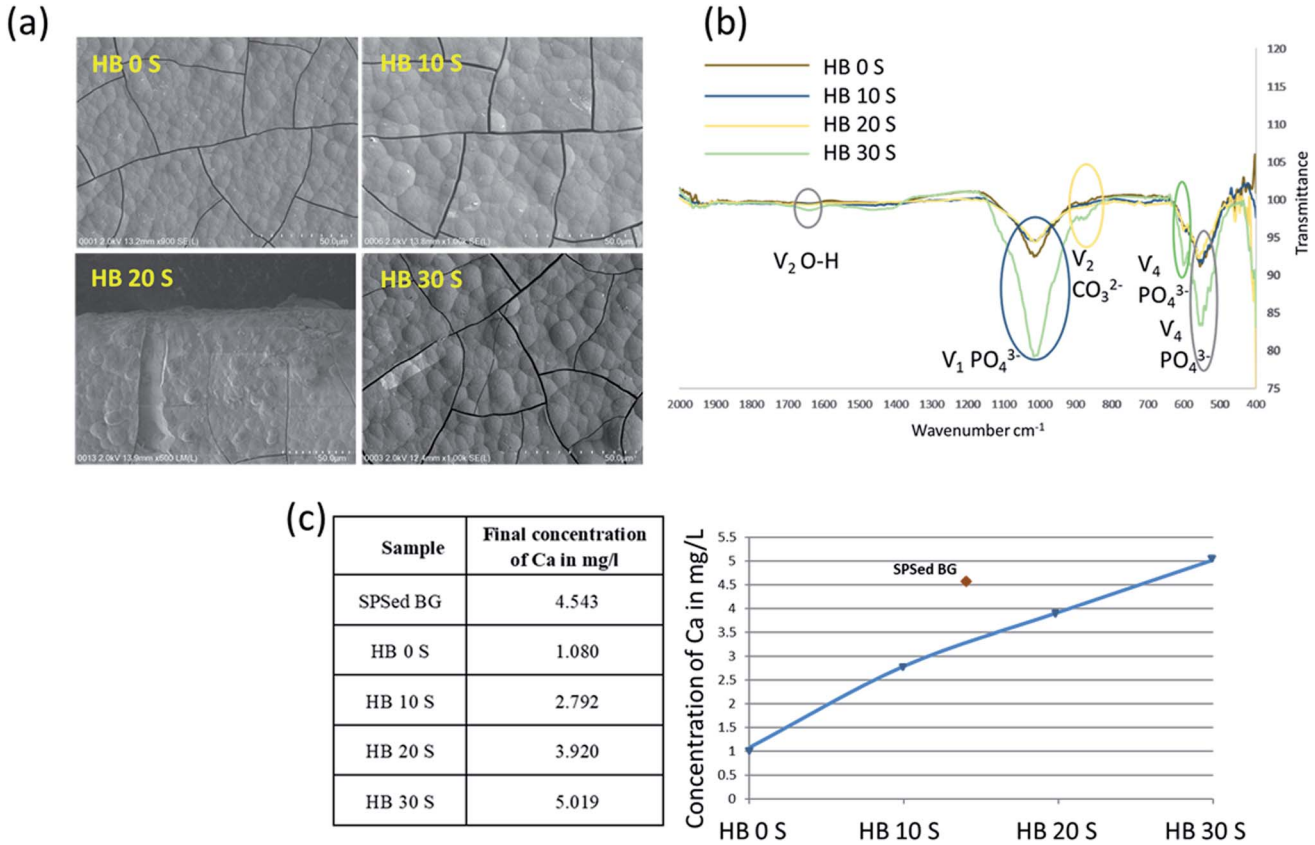

Sample	Final concentration of Ca in mg/l
SPSed BG	4.543
HB 0 S	1.080
HB 10 S	2.792
HB 20 S	3.920
HB 30 S	5.019

Fig. 2 Bioactivity characterisation of the HB 0 S, HB 10 S, HB 20 S and HB 30 S composite scaffolds based on the apatite layer on their surface. (a) FESEM micrographs of the apatite layers formed on the surface of the scaffolds, (b) FTIR spectra of the apatite layer and (c) resorption rate analysis corresponding to calcium dissolution.

observed with the *Staphylococcus* (*S.*) *epidermidis* strain (Fig. 3b and d). Incubation of *Staphylococcus* spp. with HA powder seemed to have a poor inhibition against all the bacterial strains. This observation was obvious in the *S. aureus* ATCC 811 (Fig. 3b) and *S. epidermidis* 700593 (Fig. 3c) exposed groups, where there was a significant increase in bacterial viability upon incubation with HA. A trend of increasing viability was also observed as the ratio of BG increased. *S. aureus* and *S. epidermidis* are clinically important Gram-positive bacteria, which account for the majority of osteomyelitis and implant failure,[40,41] and their risk never decreases with antibiotic prophylaxis.[42] This is mainly due to the compromised host environment from surgery and the opportunity for bacterial attachment provided by the foreign body.[43] HA is the major material used as a bone substitute in tissue engineering. However, it is limited by its ability to allow bacterial adherence and biofilm formation, further compromising antibiotic treatments.[44–47] This similar drawback was also encountered in the current study, where HA supported the viability of all the bacterial strains. This may be the reason why biofilm formation on the surface of HA-based implants is inevitable. Thus, the modulation of their hydrophobicity and chemical functionality has been suggested to reduce bacterial attachment, where phosphate-terminated compounds exhibit an anti-attachment efficacy of up to 40%.[48] Bioactive glass has previously been reported to exhibit anti-microbial activities, although its mechanism of action remains unclear.[49–51] In this study, bioactive glass was incorporated with HA to adopt this characteristic in the composite scaffolds. Overall, all the SPSed HA–BG composite scaffolds showed an inhibition property against all the *Staphylococcus* spp. compared with HB 0 S (Fig. 3). HB 10 S showed a statistically significant inhibition to *S. epidermidis* ATCC 700593 compared with the baseline control group (CTRL: LB broth without any compound) ($p < 0.01$) and comparable inhibition with BG (Fig. 3c). However, statistically significant inhibition to *S. aureus* ATCC 1749 (Fig. 3a) and *S. epidermidis* ATCC 35984 (Fig. 3d) was not achieved with the combination of BG and HA. These discrepancies in the results may be due to the differences in the bacterial products, which led to their subsequent attachment and growth. For instance, it has been previously reported that amylase-producing bacteria show significant attachment compared with a non-producing strain.[46,47] Nevertheless, more studies are necessary to confirm the observed differences.

3.4 Cell attachment and proliferation

Successful cell attachment on biomaterial scaffolds is one of the positive indications for material biocompatibility. In the present study, the SEM micrographs revealed that all the SPSed

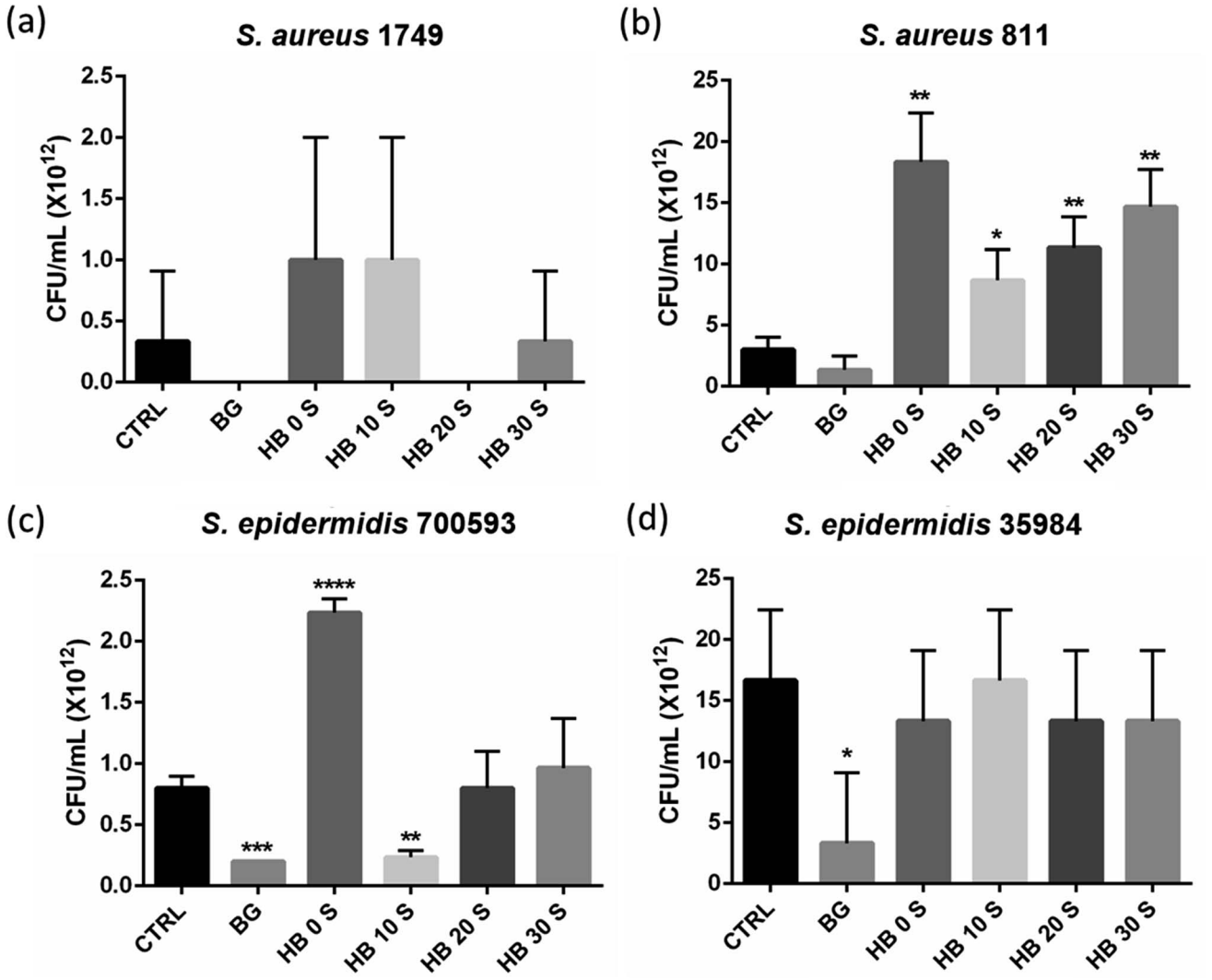

Fig. 3 Antimicrobial activity of the control, pure bioglass (BG), HB 0 S, HB 10 S, HB 20 S and HB 30 S against *Staphylococcus* spp. The viability of each bacterial strain with different combinations of HA and BG. (a) and (b) Methicillin-resistant strain. (c) and (d) Methicillin-sensitive strain. Data shown as mean ± SD from one experiment run in triplicate. Statistical significance was analysed with unpaired Student's *t*-test (*$p < 0.05$, **$p < 0.01$, ***$p < 0.001$, ****$p < 0.0001$). LB broth without any compound was used as a baseline control (CTRL), while pure bioglass (BG) powder was used as a positive control.

HA–BG composite scaffolds exhibited a high affinity for hBMSC attachment (Fig. 4a). The scaffolds without cells (bare samples) served as a baseline control. It was observed that the surface of all the scaffolds was extensively colonised by the cells. Extracellular matrix (ECM) secretion was obvious on the periphery and microenvironment of the cells, suggesting that the materials provided an optimal surface for cell attachment and adaption. In addition, it gives an indication of the osteogenic differentiation of hBMSCs. Biomaterial scaffolds for orthopaedic and dental applications should maintain cell viability and promote proliferation.[1] In the present study, the viability and proliferation of SPSed HA–BG composite scaffold-seeded hBMSCs were analysed using Alamar Blue (AB) colorimetric indicator on day 1, 3, 7, 14 and 21. The cell viability was measured relative to the percentage reduction in AB at each time point, and the proliferation was measured at different time points using day 1 as a comparison group. Cell viability of more than 40% was observed in all the samples on day 1 (Fig. 4b). An increasing trend in AB reduction was also observed from day 1 to 21, which was directly proportional to the rate of hBMSC proliferation. The cells seeded in HB 10 S and HB 20 S exhibited significantly increased AB reduction from day 1 to day 3 ($p < 0.01$). This may be due to their relatively higher porosity in these scaffolds compared to HB 0 S and HB 30 S, which provided a larger surface area for cell attachment and proliferation.[52]

3.5 *In Vitro* mineralisation

Mineralisation in the microenvironment of cells seeded on a biomaterial is an indication of the adaption of the cells to the material surface.[53] During the osteogenic differentiation of hBMSCs, the deposition of ECM commences and the cellular periphery serves as the nucleation site of the mineralized matrix.[54,55] In the present study, the intensity of Alizarin Red (AR) S staining was greater on the cell-seeded SPSed HA–BG

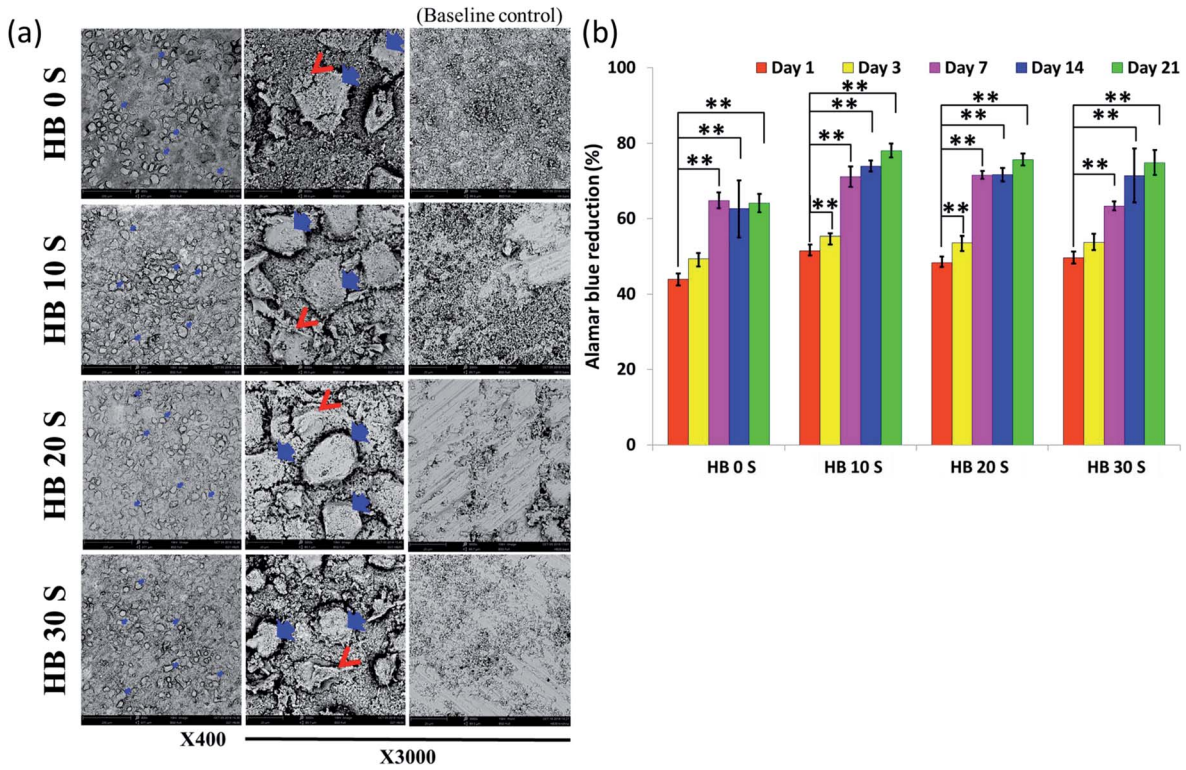

Fig. 4 Biocompatibility evaluation of HB 0 S, HB 10 S, HB 20 S and HB 30 S using hBMSCs. (a) SEM micrographs obtained at day 21 and (b) Alamar Blue (AB) cell proliferation analysis. SPSed HA–BG composite scaffolds without cells (baseline control) on day 1, 3, 7, 14 and 21. Data shown as mean ± SD from one experiment run in triplicate. Statistical analysis was performed between days (day 1, baseline control) and groups (HB 0 S, baseline control) using the Mann–Whitney and Kruskal–Wallis tests. The assessments were reported to be statistically significant if $^{**}p < 0.01$. Cell: ➡ and extracellular matrix (ECM): >.

composite scaffolds compared with the baseline control (HB 0 S) (Fig. 5a). This calcium (Ca) deposition from AR S staining was further confirmed *via* elemental analysis for Ca content on the periphery of the cells seeded on the scaffolds using EDAX. The absolute atomic concentration of Ca was calculated by eliminating the Au content. It was found that about a 1.1-, 1.3- and 1.2-fold increase in Ca concentration in HB 10 S, HB 20 S and HB 30 S, respectively, was observed compared with that of HB 0 S (Fig. 5b). This finding supports the notion that the HA–BG composite scaffolds increased the mineralisation activity of the hBMSCs with an increase in BG concentration. This observation supports the assumption that BG is beneficial for the osteogenic differentiation of hBMSCs. This phenomenon was clearly described by Maria Karadjian *et al.*, where the addition of BGs to CaPs enhanced the osteogenic differentiation of precursor cell populations in *in vitro* conditions.[56]

3.6 Osteogenic protein release

Our earlier finding demonstrated the formation of bone-like appetite on the SPSed HA–BG composite scaffolds when they were immersed in simulated body fluid, suggesting the excellent bioactivity of these composites. Osteogenic differentiation and mineralised matrix secretion involve the expression of an array of genes and proteins, which that guide this mechanism.[57] To explore the role of the SPSed HA–BG composite scaffolds in hBMSC osteogenic differentiation, several osteogenic-related markers were investigated at different time points. ALP and OC are time-dependent osteoblast markers, which specify the osteogenic differentiation pattern of hBMSCs.[32] Overall, an increasing trend of ALP activity was observed from the cells seeded on the SPSed HA–BG composite scaffolds (Fig. 6a). Interestingly, the HB 30 S-seeded cells showed a significant increase in ALP catalysis with an average of 1.8-fold higher activity compared to that of the HB 0 S-seeded cells on day 5, 15 and 20 ($p < 0.05$). This observation proved the fact that the osteogenic differentiation process in the hBMSCs seeded on the HB 30 S scaffold occurred within a suitable time.

OC is a protein matrix that occupies 20% of the total non-collagenous composition of bone.[58] This protein is secreted primarily by osteoblasts during mineralisation activity, thus it is identified as a late-stage osteoblast differentiation marker.[59] In the present study, the OC secretion by the cells seeded on the HB 30 S scaffold demonstrated an increasing trend at different time points (Fig. 6b). This secretion was statistically significant on day 15 (2.39 ng mL^{-1}, $p < 0.01$) when compared with that of HB 0 S (2.21 ng mL^{-1}). Based on the intact release of OC in the culture media, it can be inferred that the hBMSCs seeded on the HB 30 S scaffold underwent significant osteogenic differentiation. This finding is also in agreement with the observation reported by CaiXia Xu and colleagues. They found an increasing

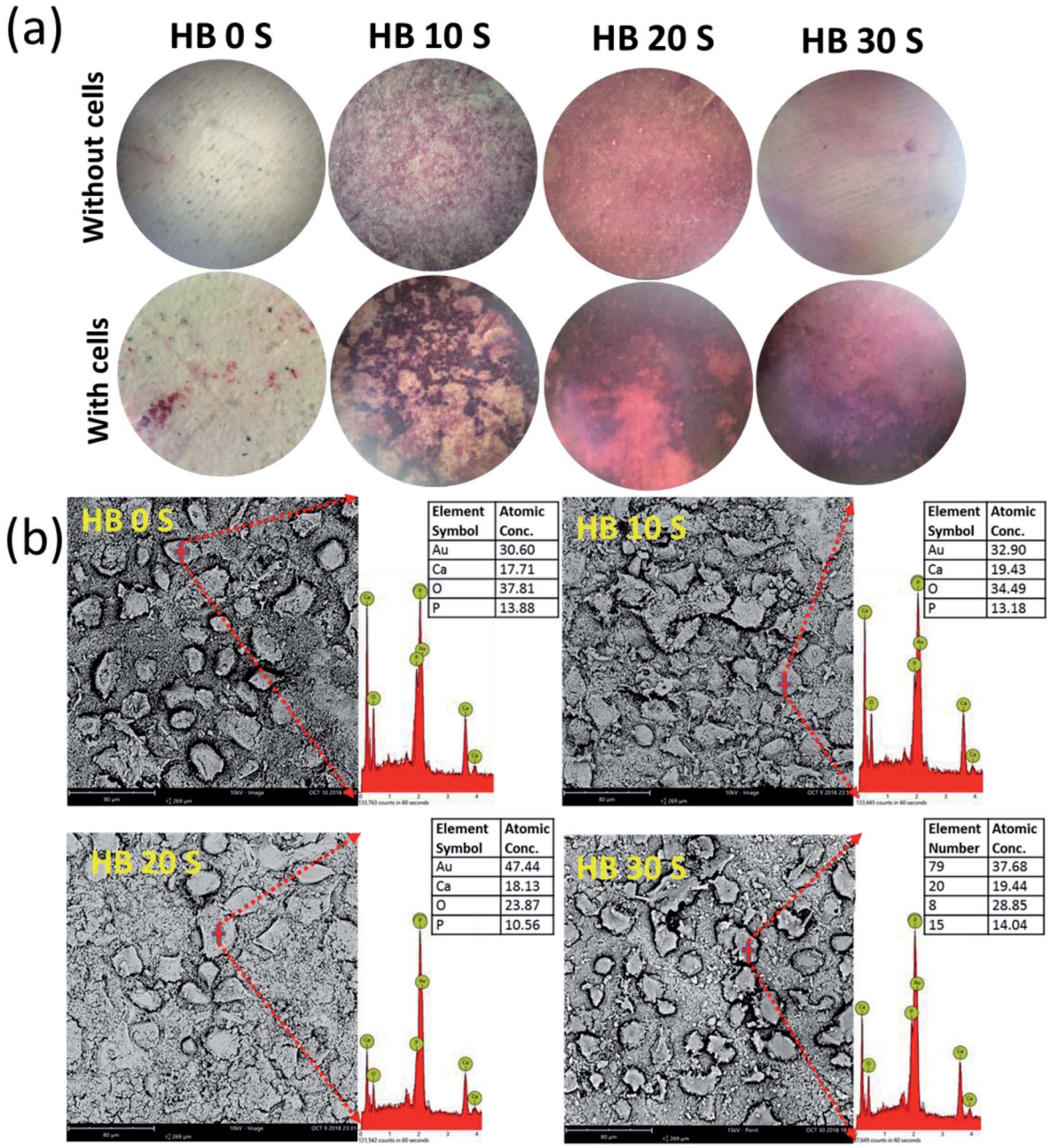

Fig. 5 Mineralisation/calcium deposition process on the periphery of the seeded hBMSCs on HB 0 S, HB 10 S, HB 20 S and HB 30 S. (a) Alizarin Red (AR) S staining and (b) EDAX. The cell-free scaffold was used as a baseline control.

trend in OC release from day 1 up to day 14 from rat bone marrow-derived MSCs when they were seeded on a collagen–phosphatidylserine scaffold incorporated with bioglass.[60]

3.7 Osteogenic intra- and extra-cellular proteins

Bone morphogenetic protein (BMP) is a multifunctional acidic polypeptide, which is primarily secreted and synthesised by osteoblast cells.[61] Currently, more than 20 subtypes of BMP have been discovered, but among them, BMP2 is the most significant osteoinductive factor.[62] The role of BMP2 is to induce the differentiation of mesenchymal stem cells into bone or cartilage.[63] A higher BMP2 expression corresponds to an increase in the osteoinductive capacity of CaP ceramics.[64] In the present study, the localised secretion of BMP2 was the most vibrant on the HB 30 S-seeded cells compared with HB 0 S, HB10 S and HB 20 S (Fig. 7a and S3a†). This red fluorescence intensity in HB 30 S was statistically significant ($p < 0.01$) with a 3-fold in increase compared with that of HB 0 S (Fig. 7d). This finding clearly suggests that BG supports the osteogenic differentiation of hBMSCs. It was suggested earlier that BG has potential to upregulate the BMP2 pathway in mesenchymal stem cells (MSCs).[65] This may be one of the reasons why enhanced BMP2 secretion was observed in the hBMSCs seeded on HB 30 S in the absence of osteogenic factors from the culture media.

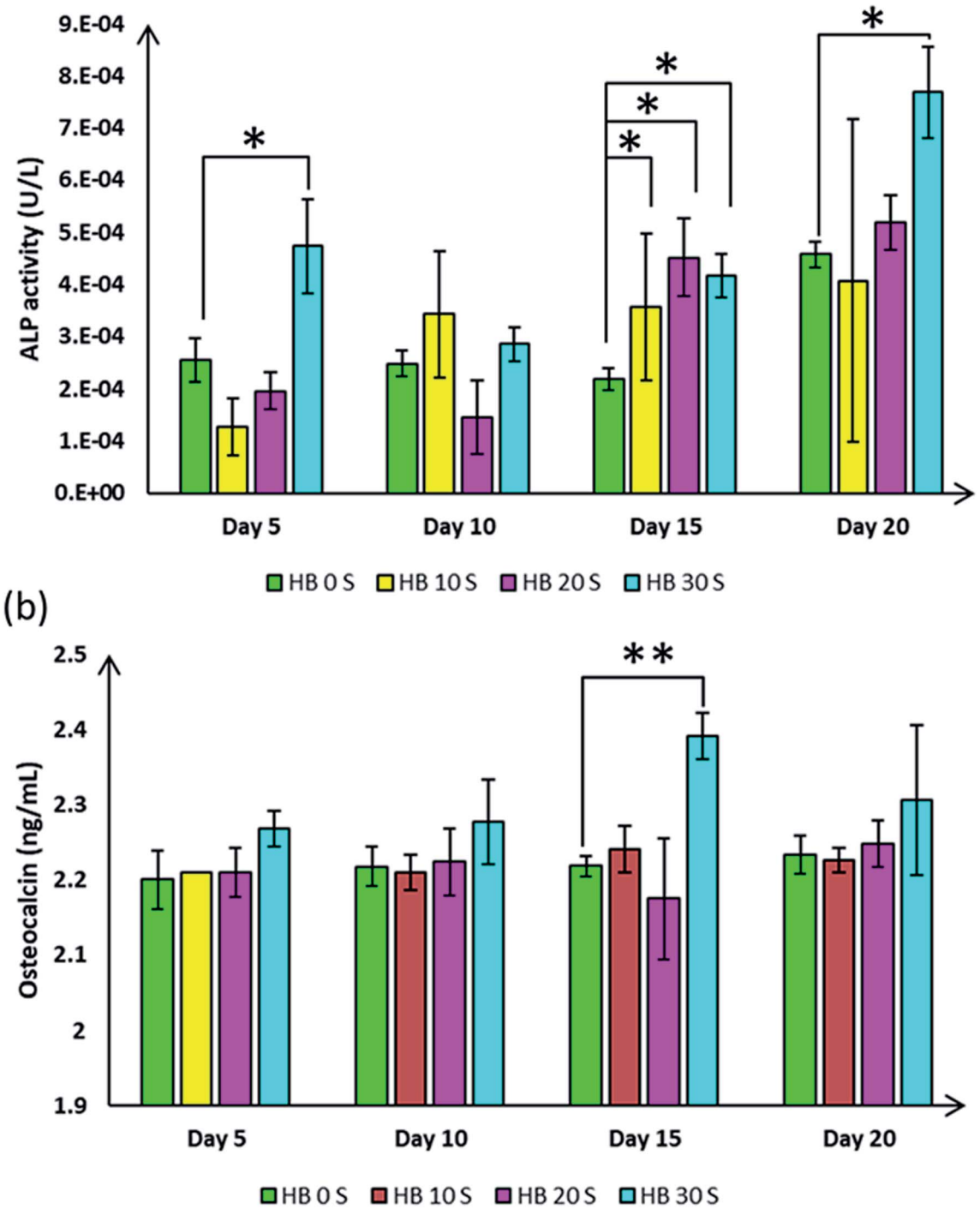

Fig. 6 ELISA assays on media harvested from the culture of hBMSC-seeded HB 0 S, HB 10 S, HB 20 S or HB 30 S on day 5, 10, 15 and 20. (a) Alkaline phosphatase (ALP) and (b) osteocalcin (OC). Statistical analysis was performed between days (day 5, baseline control) and groups (HB 0 S, baseline control) using the Mann–Whitney and Kruskal–Wallis tests in SPSS. The assessments were reported to be statistically significant if *p < 0.05 and **p < 0.01.

Type-1 collagen (COL1) is the most abundant protein found in the ECM of bony tissues[66] and bone is the main factory for the synthesis of collagen.[67] The secretion of COL1 was obvious on the periphery of the cells seeded on all the HA–BG scaffold types (Fig. 7b and S3b†). The intensity of the COL1 secretion was statistically significant on both the HB 20 S- and HB 30 S-seeded cells (p < 0.01), but not on the HB 10 S-seeded cells (Fig. 7d). However, this discrepancy is not clearly understood. In previous studies, collagen was used either as a culture dish coating or in 3D gel format to induce the osteogenic differentiation of hBMSCs.[68] In the present study, COL1 secretion without exogenous type-1 collagen molecules in the media was observed. This indicates that the hBMSCs could be well adapted on the surface of the SPSed HA–BG composite scaffolds. Furthermore,

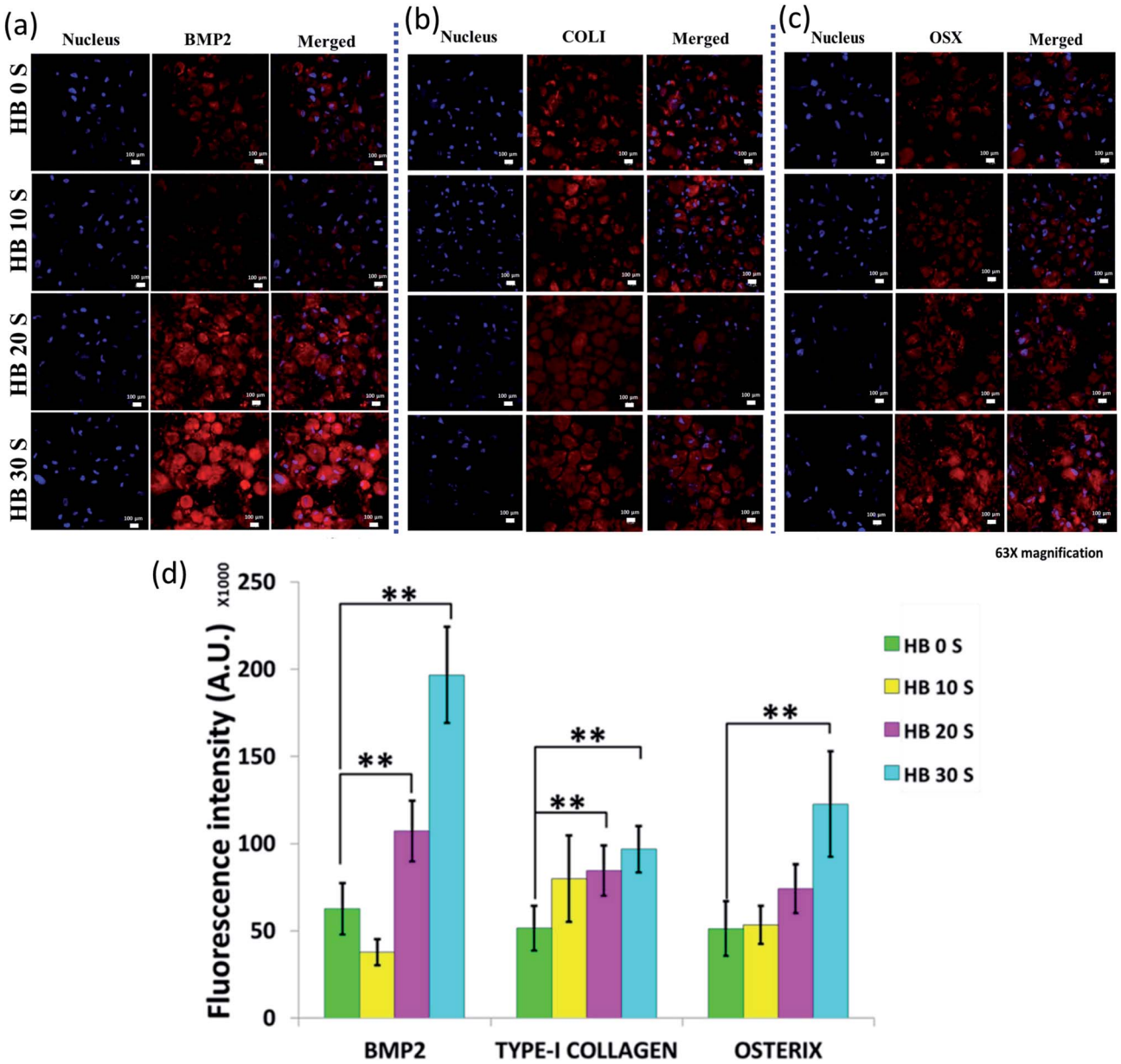

Fig. 7 Immunocytochemistry of intra- and/or extra-cellular proteins and imaging using confocal laser scanning microscopy (CLSM). (a) Bone morphogenetic protein-2 (BMP2), (b) Type-1 collagen (COL1), (c) Osterix (OSX) and (d) corrected total cell fluorescence intensity (CTCF). Data is presented as the mean ± standard deviation. Statistical analysis was performed between groups (HB 0 S, baseline control) using Mann–Whitney and Kruskal–Wallis tests in SPSS. The assessments were reported statistically significant if $^{**}p < 0.01$.

these cells seemed to create a microenvironment favourable for osteogenic differentiation and matrix mineralisation with COL1 deposition.[69] This was well supported by the SEM micrographs of the hBMSCs, with noticeable ECM on the cellular periphery and surroundings.

Osterix (OSX) is a zinc finger-containing transcription factor, which is an essential protein for osteoblast differentiation during the bone development process.[70,71] OSX is an indicator for the differentiation of pre-osteoblasts into mature osteoblasts and/or osteocytes.[72] The OSX intracellular expression in the HB 30 S-seeded cells significantly increased by 2.4-fold compared with that of HB 0 S ($p < 0.01$) (Fig. 7c and d and S3c†). This amplified OSX expression may be associated with the presence of an increased glassy phase (Si) and enhanced Ca dissolution in HB 30 S. This was supported by a previous finding, where commercial Bioglass™ (45S5)-conditioned media significantly induced OSX and osteogenic differentiation of the MC3T3-E1 calvaria cell line.[73]

3.8 Monocyte migration analysis

A scaffold *in vivo* must overcome the challenges from immune cells, which guard the host cells from any type of assault derived from foreign bodies. These immune cells including monocytes/macrophages as frontline sentinel cells can reject a foreign body if it found to be a threat to the host cells.[74] This foreign body

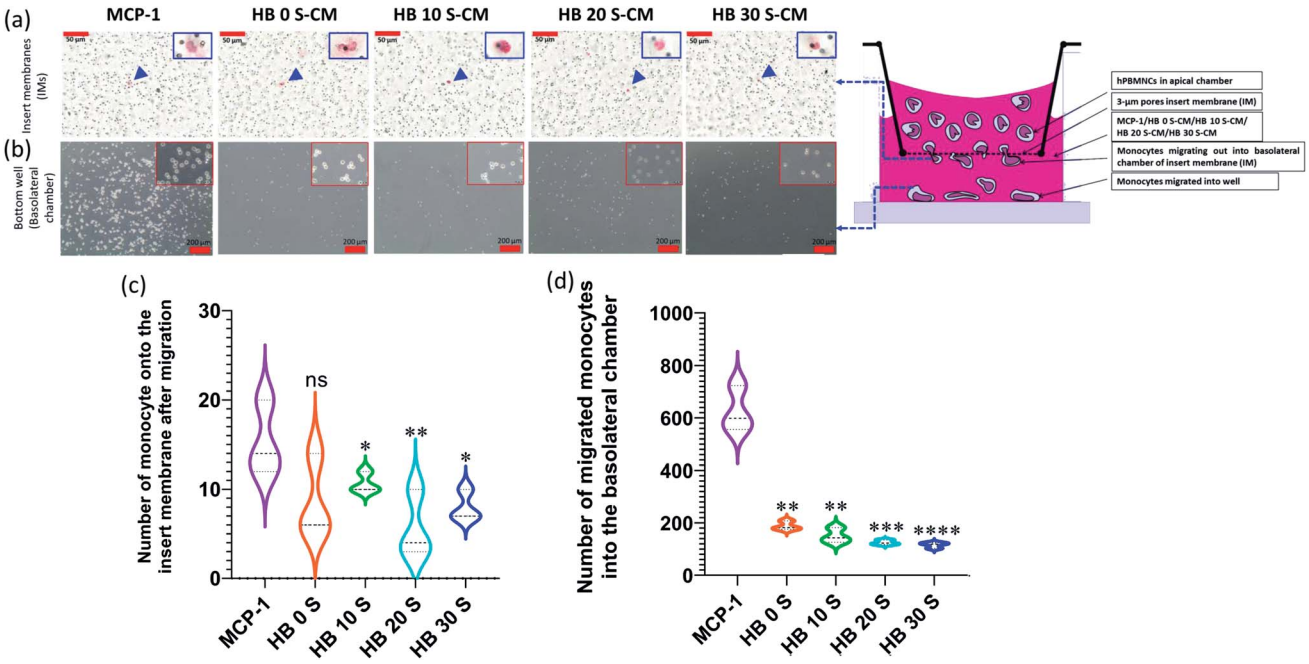

Fig. 8 Monocyte migration in response to monocyte chemoattractant protein-1 (MCP-1, positive control), HB 0 S-CM, HB 10 S-CM, HB 20 S-CM and HB 30 S-CM. (a) Monocytes migrating from 3 μm pore size transwell insert membranes (IM), (b) bright-field images of migrated monocytes in basolateral chamber, (c) migrated monocyte count from six randomly selected areas on the IM and (d) basolateral migrated monocyte count from the bright-field images using the Image-J analysis tool. Statistical analysis was performed between groups (MCP-1, positive control) using the Mann–Whitney and Kruskal–Wallis tests in SPSS. The assessments were reported to be statistically significant if $*p < 0.05$, $**p < 0.01$, $***p < 0.001$ or $****p < 0.0001$.

reaction can be initiated by the intrinsic characteristics of scaffolds including their chemical composition, dimension, pore size and surface topography.[75] Therefore, understanding the level foreign body reaction of novel biomaterial scaffolds will provide a clue to improve their characteristics before considering them for implantation. In the present study, the immune cell response to the SPSed HA–BG composite scaffolds was investigated using a 3 μm pore size insert membrane (IM) transwell model mimicking the microenvironment at the bone–implant interface. The monocytes were challenged with the composite scaffolds to prepare HA–BG-conditioned medium, which contained mediators such as pro-inflammatory cytokines/chemokine as a result of the interaction of monocytes with the scaffolds. This conditioned medium, which mimics local tissue inflammation, was used to understand the response of circulating monocytes in the blood in terms of their migration activity. Monocytes with a kidney bean-shaped nucleus were randomly found migrating into the basolateral site of the insert membrane (IM) through the 3 μm pores in response to the HA–BG-conditioned medium, but this migration was significant in the MCP-1-treated well ($*p < 0.05$ or $**p < 0.01$) (Fig. 8a and c and S4†). A similar scenario was observed in the lower/basolateral well, where significant migration was observed in the positive control (MCP-1) but not in response to the HA–BG-conditioned medium (Fig. 8b and d and S5†). This finding is consistent with a previous study, where monocyte-derived macrophages were significantly polarised with a lipopolysaccharide (LPS)/interferon-gamma (IFN-γ)-treated well but not with bioactive glass.[76] Furthermore, this is the first study to investigate the monocyte migration in response to HA–BG-conditioned medium mimicking the microenvironment at the bone–scaffold interface during post-operative recovery after implantation.

4 Conclusion

Composite scaffolds were prepared using a novel set of SPS processing parameters, which successfully avoided the formation of undesirable phases. Due to the formation of only CaP phases and bioactive glassy regions, desirable physicochemical behaviour and stable bioactive responses were achieved. These findings suggest that the HA–BG scaffolds can support bone mineralisation. Furthermore, antimicrobial behaviour, which plays a crucial role in the early stages of scaffold implantation, was also observed against *Staphylococcus* spp. Promising hBMSC attachment and proliferation and osteoinductive characteristics without the presence of exogenous osteogenic factors were also exhibited by all the sample groups, especially HB 30 S. In addition, these composite scaffolds also exhibited resistance to monocyte migration, suggesting their behaviour to escape a foreign body reaction. Thus, based on the physicochemical and *in vitro* biological results, the SPSed HA–BG composite scaffolds are potential substitutes for bone grafts in treating bone defects. However, according to the standard protocol, pre-clinical animal trials must be immediately performed before these scaffolds can qualify for clinical trials.

Author contributions

M. H. and T. K. supervised the study. M. R. and K. G. conceptualized, analysed data, investigated and wrote the original draft. A. M., T. K. and W. J. B. acquired the funding. M. R., K. G., R. A., M. M. R. and H. R. B. contributed to the methodology. Y. Y. C. and W. F. W. performed antimicrobial experiments. All authors have given approval to the final version of the manuscript.

Funding sources

Fundamental Research Grant Scheme (FRGS) – FRGS/1/2016/SKK08/UM/02/20.

Data availability

The raw data required to reproduce these findings are available to download from [https://data.mendeley.com/datasets/9ggjb2bxfs/2].

Conflicts of interest

The authors declare no competing financial interest.

Acknowledgements

We are thankful to Professor Katsuyoshi Kondoh for allowing us to carry out Spark Plasma Sintering technique for SPSed HA–BG composited scaffolds fabrication at his lab, Joining and Welding Research Institute Osaka University, Japan.

References

1 G. Krishnamurithy, M. R. Murali, M. Hamdi, A. A. Abbas, H. B. Raghavendran and T. Kamarul, *Ceram. Int.*, 2014, **40**, 771–777.
2 G. Wypych, in *Functional Fillers*, ChemTec Publishing, 2018, pp. 153–179.
3 M. Rizwan, M. Hamdi and W. J. Basirun, *J. Biomed. Mater. Res., Part A*, 2017, **105**, 3197–3223.
4 K. Lawton, H. Le, C. Tredwin and R. D. Handy, *Int. J. Nanomed.*, 2019, **14**, 7947.
5 S. Baradaran, E. Moghaddam, B. Nasiri-Tabrizi, W. J. Basirun, M. Mehrali, M. Sookhakian, M. Hamdi and Y. Alias, *Mater. Sci. Eng., C*, 2015, **49**, 656–668.
6 S. El-Tablawy, W. Abd-Allah and E. Araby, *Silicon*, 2018, **10**, 931–942.
7 A. Tavakolizadeh, M. Ahmadian, M. H. Fathi, A. Doostmohammadi, E. Seyedjafari and A. Ardeshirylajimi, *ASAIO J.*, 2017, **63**, 512–517.
8 X. Liu, M. N. Rahaman, G. E. Hilmas and B. S. Bal, *Acta Biomater.*, 2013, **9**, 7025–7034.
9 M. Rizwan, M. Hamdi, W. J. Basirun, K. Kondoh and J. Umeda, *Ceram. Int.*, 2018, **44**, 23052–23062.
10 M. K. Yadav, J. E. Vidal and J.-J. Song, in *New and Future Developments in Microbial Biotechnology and Bioengineering: Microbial Biofilms*, Elsevier, 2020, pp. 15–28.
11 J. R. Mauney, V. Volloch and D. L. Kaplan, *Tissue Eng.*, 2005, **11**, 787–802.
12 E. Birmingham, G. L. Niebur, P. E. McHugh, G. Shaw, F. P. Barry and L. M. McNamara, *Eur. Cells Mater.*, 2012, **23**, 13–27.
13 F. Paino, M. La Noce, A. Giuliani, A. De Rosa, S. Mazzoni, L. Laino, E. Amler, G. Papaccio, V. Desiderio and V. Tirino, *Clin. Sci.*, 2017, **131**, 699.
14 D.-F. Zhao, C.-L. Wang and Y.-J. Zhao, *World J. Tradit. Chin. Med.*, 2015, **1**, 50–55.
15 T. Ma, *J. Mater. Chem. B*, 2014, **2**, 31–35.
16 E. Mariani, G. Lisignoli, R. M. Borzi and L. Pulsatelli, *Int. J. Mol. Sci.*, 2019, **20**, 636.
17 S. Metwally and U. Stachewicz, *Mater. Sci. Eng., C*, 2019, **104**, 109883.
18 T. Kokubo and H. Takadama, *Biomaterials*, 2006, **27**, 2907–2915.
19 G. Rh Owen, M. Dard and H. Larjava, *J. Biomed. Mater. Res., Part B*, 2018, **106**, 2493–2512.
20 A. Ito, Y. Sogo, A. Yamazaki, M. Aizawa, A. Osaka, S. Hayakawa, M. Kikuchi, K. Yamashita, Y. Tanaka and M. Tadokoro, *Acta Biomater.*, 2015, **25**, 347–355.
21 T. Waltimo, T. J. Brunner, M. Vollenweider, W. J. Stark and M. Zehnder, *J. Dent. Res.*, 2007, **86**, 754–757.
22 H. R. Balaji Raghavendran, S. Puvaneswary, S. Talebian, M. Raman Murali, S. Vasudevaraj Naveen, G. Krishnamurithy, R. McKean and T. Kamarul, *PLoS One*, 2014, **9**, e104389.
23 G. Krishnamurithy, N. A. Yahya, M. Mehrali, M. Mehrali, S. Mohan, M. R. Murali, H. R. B. Raghavendran and T. Kamarul, *Ceram. Int.*, 2016, **42**, 18247–18256.
24 A. Cuccu, S. Montinaro, R. Orru, G. Cao, D. Bellucci, A. Sola and V. Cannillo, *Ceram. Int.*, 2015, **41**, 725–736.
25 H. S. Ryu, H. J. Youn, K. S. Hong, B. S. Chang, C. K. Lee and S. S. Chung, *Biomaterials*, 2002, **23**, 909–914.
26 D. Bellucci, R. Salvatori, M. Cannio, M. Luginina, R. Orrù, S. Montinaro, A. Anesi, L. Chiarini, G. Cao and V. Cannillo, *Biomed. Glas.*, 2018, **4**, 21–31.
27 H. Demirkiran, Y. Hu, L. Zuin, N. Appathurai and P. B. Aswath, *J. Mater. Sci.*, 2011, **31**, 134–143.
28 R. Karan, P. Manna, P. K. Maiti and K. Das, *J. Aust. Ceram. Soc.*, 2020, 1–11.
29 M. Vallet-Regi, *Bio-ceramics with clinical applications*, John Wiley & Sons, 2014.
30 A. Hoppe, N. S. Güldal and A. R. J. B. Boccaccini, *Biomaterials*, 2011, **32**, 2757–2774.
31 I. Junkar, in *Advances in Biomembranes and Lipid Self-Assembly*, ed. A. Iglič, C. V. Kulkarni and M. Rappolt, Academic Press, 2016, vol. 23, pp. 25–59.
32 G. Krishnamurithy, M. R. Murali, M. Hamdi, A. A. Abbas, H. B. Raghavendran and T. Kamarul, *Regener. Med.*, 2015, **10**, 579–590.
33 G. Krishnamurithy, N. A. Yahya, M. Mehrali, M. Mehrali, S. Mohan, M. R. Murali, H. R. B. Raghavendran and T. Kamarul, *Ceram. Int.*, 2016, **42**, 18247–18256.
34 C. Drouet, *BioMed Res. Int.*, 2013, 1–12.

35 K. Rezwan, Q. Chen, J. Blaker and A. R. Boccaccini, *Biomaterials*, 2006, **27**, 3413–3431.
36 M. T. Islam, R. M. Felfel, E. A. Abou Neel, D. M. Grant, I. Ahmed and K. M. Z. Hossain, *J. Tissue Eng.*, 2017, **8**, 2041731417719170.
37 I. V. Pylypchuk, A. Petranovskaya, P. Gorbyk, A. Korduban, P. Markovsky and O. Ivasishin, *Nanoscale Res. Lett.*, 2015, **10**, 338.
38 P. Habibovic, F. Barrere, C. A. Blitterswijk, K. Groot and P. Layrolle, *J. Am. Ceram. Soc.*, 2002, **85**, 517–522.
39 S. V. Dorozhkin, *Biomaterials*, 2010, **31**, 1465–1485.
40 A. Becker, C. Triffault-Fillit, F. Valour, L. Boussel, A. Ruffion, F. Laurent, E. Senneville, C. Chidiac and T. Ferry, *Médecine et Maladies Infectieuses*, 2019.
41 P. Doshi, H. Gopalan, S. Sprague, C. Pradhan, S. Kulkarni and M. Bhandari, *BMC Musculoskeletal Disord.*, 2017, **18**, 156.
42 M. Backes, S. A. Dingemans, M. G. W. Dijkgraaf, H. R. van den Berg, B. van Dijkman, J. M. Hoogendoorn, P. Joosse, E. D. Ritchie, W. H. Roerdink, J. P. M. Schots, N. L. Sosef, I. J. B. Spijkerman, B. A. Twigt, A. H. van der Veen, R. N. van Veen, J. Vermeulen, D. I. Vos, J. Winkelhagen, J. C. Goslings and T. Schepers, *Jama*, 2017, **318**, 2438–2445.
43 W. Zimmerli, *J. Intern. Med.*, 2014, **276**, 111–119.
44 W. B. Clark, L. L. Bammann and R. J. Gibbons, *Infect. Immun.*, 1978, **19**, 846–853.
45 A. Ganguli, C. Steward, S. L. Butler, G. J. Philips, S. T. Meikle, A. W. Lloyd and M. H. Grant, *J. Mater. Sci.: Mater. Med.*, 2005, **16**, 283–287.
46 J. D. Rogers, R. J. Palmer, P. E. Kolenbrander and F. A. Scannapieco, *Infect. Immun.*, 2001, **69**, 7046.
47 F. A. Scannapieco, G. I. Torres and M. J. Levine, *J. Dent. Res.*, 1995, **74**, 1360–1366.
48 J. Marine, C. P. Myers, G. A. Picquet, L. A. Zaidel, D. Wu and K. E. Uhrich, *Colloids Surf., B*, 2018, **167**, 531–537.
49 S. Kaya, M. Cresswell and A. R. Boccaccini, *Mater. Sci. Eng., C*, 2018, **83**, 99–107.
50 J. Li, D. Zhai, F. Lv, Q. Yu, H. Ma, J. Yin, Z. Yi, M. Liu, J. Chang and C. Wu, *Acta Biomater.*, 2016, **36**, 254–266.
51 J. S. Fernandes, P. Gentile, R. A. Pires, R. L. Reis and P. V. Hatton, *Acta Biomater.*, 2017, **59**, 2–11.
52 V. Karageorgiou and D. Kaplan, *Biomaterials*, 2005, **26**, 5474–5491.
53 R. Fliefel, C. Popov, M. Tröltzsch, J. Kühnisch, M. Ehrenfeld and S. Otto, *J. Craniomaxillofac. Surg.*, 2016, **44**, 715–724.
54 J. Grzesiak, A. Śmieszek and K. Marycz, *Cell Biosci.*, 2017, **7**, 2.
55 N. E. Vrana and K. Iniewski, *Biomaterials and Immune Response: Complications, Mechanisms and Immunomodulation*, ed. N. E. Vrana, CRC Press, 2018, p. 294.
56 M. Karadjian, C. Essers, S. Tsitlakidis, B. Reible, A. Moghaddam, A. R. Boccaccini and F. Westhauser, *Int. J. Mol. Sci.*, 2019, **20**, 305.
57 P. Naddeo, L. Laino, M. La Noce, A. Piattelli, A. De Rosa, G. Iezzi, G. Laino, F. Paino, G. Papaccio and V. Tirino, *Dental materials Academy of Dental Materials*, 2015, **31**, 235–243.
58 G. Krishnamurithy, S. Mohan, N. A. Yahya, A. Mansor, M. R. Murali, H. R. B. Raghavendran, R. Choudhary, S. Sasikumar and T. Kamarul, *PLoS One*, 2019, **14**, e0214212.
59 T. Cundy, I. R. Reid and A. Grey, in *Clinical Biochemistry: Metabolic and Clinical Aspects*, ed. M. Lapsley, A. P. Day and R. M. Ayling, Churchill Livingstone, 3rd edn, 2014, pp. 604–635.
60 C. Xu, P. Su, X. Chen, Y. Meng, W. Yu, A. P. Xiang and Y. Wang, *Biomaterials*, 2011, **32**, 1051–1058.
61 J. Sun, J. Li, C. Li and Y. Yu, *Mol. Med. Rep.*, 2015, **12**, 4230–4237.
62 T. Date, Y. Doiguchi, M. Nobuta and H. Shindo, *J. Orthop. Sci.*, 2004, **9**, 503–508.
63 S. Khosla, J. J. Westendorf and M. J. Oursler, *J. Clin. Invest.*, 2008, **118**, 421–428.
64 Z. Tang, X. Li, Y. Tan, H. Fan and X. Zhang, *Regener. Biomater.*, 2017, **5**, 43–59.
65 S. Midha, S. Kumar, A. Sharma, K. Kaur, X. Shi, P. Naruphontjirakul, J. R. Jones and S. Ghosh, *Biomed. Mater.*, 2018, **13**, 055012.
66 C. Granéli, A. Thorfve, U. Ruetschi, H. Brisby, P. Thomsen, A. Lindahl and C. Karlsson, *Stem Cell Res.*, 2014, **12**, 153–165.
67 N. Shaw and W. Högler, in *Pediatric Bone*, Elsevier, 2nd edn, 2012, pp. 361–381.
68 A. W. Lund, J. P. Stegemann and G. E. Plopper, *Open Stem Cell J.*, 2009, **1**, 40–53.
69 T. Kihara, M. Hirose, A. Oshima and H. Ohgushi, *Biochem. Biophys. Res. Commun.*, 2006, **341**, 1029–1035.
70 K. Nakashima, X. Zhou, G. Kunkel, Z. Zhang, J. M. Deng, R. R. Behringer and B. de Crombrugghe, *Cell*, 2002, **108**, 17–29.
71 Y. Cao, Z. Zhou, B. de Crombrugghe, K. Nakashima, H. Guan, X. Duan, S.-F. Jia and E. S. Kleinerman, *Cancer Res.*, 2005, **65**, 1124–1128.
72 K. M. Sinha and X. Zhou, *J. Cell. Biochem.*, 2013, **114**, 975–984.
73 V. G. Varanasi, T. Odatsu, T. Bishop, J. Chang, J. Owyoung and P. M. Loomer, *J. Biomed. Mater. Res., Part A*, 2016, **104**, 2604–2615.
74 Z. Sheikh, P. J. Brooks, O. Barzilay, N. Fine and M. Glogauer, *Materials*, 2015, **8**, 5671–5701.
75 G. S. A. Boersema, N. Grotenhuis, Y. Bayon, J. F. Lange and Y. M. Bastiaansen-Jenniskens, *BioRes. Open Access*, 2016, **5**, 6–14.
76 N. Gomez-Cerezo, L. Casarrubios, I. Morales, M. J. Feito, M. Vallet-Regi, D. Arcos and M. T. Portoles, *J. Colloid Interface Sci.*, 2018, **528**, 309–320.

